Environmental Fluid Mechanics Laboratory
Department of Civil Engineering
Stanford University
Stanford, California 94305-4020

Solution of Mean Flow Profiles for a Stratified Two-Phase Flow using the K-Epsilon Turbulence Model

A Final Report on
A Study of the Surface Layers at an Air-Water Interface

by
Jonathan A. Harris
and
Robert L. Street

Report EFML 91-1
November 1991

This research was sponsored by
The Fluid Dynamics Program
Mechanics Division
Office of Naval Research
Grant N00014-90-J-1294

Preface

This paper is the final report for and describes the work accomplished under Grant No. N00014-90-J-1294 from the Fluid Dynamics Program, Mechanics Division, Office of Naval Research. The purpose of the grant was to support research on a study of the surface layers at an air-water interface. The period of the research was 15 November 1989 through 15 February 1991.

There are no other publications completed under this grant; however, this paper is being submitted for refereed publication.

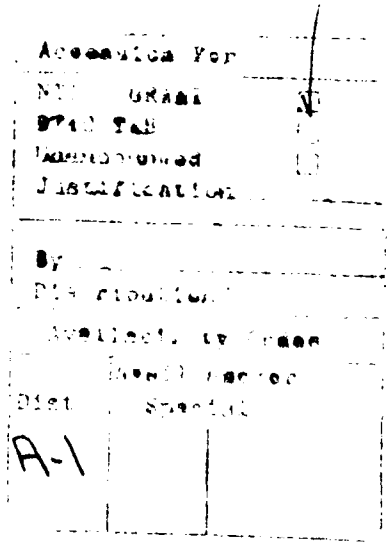

Acknowledgments

The authors would like to thank the Fluid Dynamics Program, Mechanics Division, Office of Naval Research for their finanical support under Grant No. N00014-90-J-1294.

The mathematical manipulations and generation of FORTRAN code were greatly facilitated by the use of the symbolic manipulation program *Mathematica*^{TM} running on a NeXT^{TM} workstation.

Contents

List of Figures

1 Introduction

This paper describes the application of a two-equation turbulence model to a stratified two-phase channel flow as part of a research project into wave generation by wind. The project was prompted by a review of wave-generation literature whose purpose was to determine the extent of the agreement between extant theory and observations of wave growth.

The literature review revealed that wind-generated waves may broadly be divided on the basis of u_*/c, i.e., the ratio of the friction velocity, u_*, to the wave celerity, c. Waves with values of $u_*/c \geq 0.15$ may be termed "short waves", and waves with $u_*/c \leq 0.15$ may be termed "long waves". The short wave classification includes gravity-capillary waves and most wind-waves generated in laboratory facilities. The long wave classification includes most wind-generated waves in the ocean, as well as artificially generated progressive waves over which wind is blown in laboratory facilities.

It was found that the growth of short waves is quite well described by existing wave generation theories and numerical models. For example, Valenzuela (1976) and Kawai (1979) found very good agreement between their experimental measurements of the growth of gravity-capillary waves and the predictions of viscous linear stability theory.

However, the growth of long waves is only poorly described by extant theory and numerical models. For example, wave growth rates predicted by Miles' (1957, 1959) inviscid linear instability theory are generally 2 to 5 times smaller than the most reliable experimental measurements. Various modifications to Miles' original theory have improved the agreement between theory and experiment somewhat. For example, Al-Zanaidi and Hui (1984) found that the inclusion of the wave-induced Reynolds stresses in their numerical model increased the predicted wave growth rates by up to 50% in some cases. However, the agreement between theoretical predictions and experimental measurements is still poor.

Interestingly, there is very good agreement between Miles' inviscid linear stability theory and the results of experimental and numerical studies of the flow over solid, but progressive, monochromatic waves (see, for example, Zagustin et al., 1968 and Norris and Reynolds, 1975). The most important physical difference between the flow over an artificial waveform and the flow over wind-generated water waves is that there is motion in the water under an actual wind wave, whereas an artificial waveform has a solid boundary. This observation suggests that the shear flow in the water is important for the growth of long waves. Other evidence also points to the importance of the shear flow in the water for long wave growth. For example, Valenzuela (1976) demonstrated the importance of the shear flow in the water for gravity-capillary (short) waves. He solved the coupled air-water problem (neglecting turbulent effects), and found that the inclusion of the shear flow in the water produced a significant increase in computed growth rates, especially for the waves with the lowest values of u_*/c (i.e., waves closest to the long wave

classification). Gent and Taylor (1977) found that the inclusion of the surface drift in their numerical model of wave growth significantly altered the surface pressure distribution, but only produced a slight increase in the wave growth rate. However, they only considered two different cases, and so the question remains as to whether the wave growth rate could change significantly if a larger range of wave parameters was examined. Thus, it seems likely that the inclusion of the shear flow in the water in a numerical model of the growth of long waves will increase the wave growth rate, which would improve the agreement between theoretical predictions and experimental measurements of wave growth.

A research program is currently underway to develop a comprehensive numerical model of wave growth. The aim of the model is to adequately predict the growth rates of both short and long waves. The model will solve the coupled air-water wave growth problem, and will consider the shear flow in the water as well as including turbulence effects. As such, the model will be an extension of previous numerical models of wave growth.

The numerical model is of the linear stability type, similar to most models of wave growth (e.g., Miles, Al-Zanaidi and Hui, and Valenzuela). Such models solve for perturbations to a given mean flow profile caused by a single wave component. The resulting perturbation pressure and velocity components may be used to compute the wave growth rate and other quantities of interest.

The numerical model is developed in two parts. The first involves developing a solution for the equations governing the mean flow, and the second part involves solving the perturbation problem. While these two parts are essentially separate problems, it is important to consider the solution of the mean flow part in the context of the overall model. This paper describes only the successful solution of the mean flow problem.

Many previous models of wave growth simply specify the mean velocity profile analytically. For example, Miles (1957, 1959) considered a logarithmic velocity profile in the air and ignored the flow in the water, whereas Valenzuela (1976) used a more realistic linear-logarithmic profile in the air and the water. However, the inclusion of turbulence effects in our model requires that mean profiles of turbulent quantities, as well as the velocity, must be provided as input to the perturbation problem. Thus, the analytical specification of the mean profiles is out of the question for our problem, and it is essential to solve the equations governing the turbulence and the mean flow numerically.

It is well known that the mean flow profile can have a large effect on the computed growth rate. For example, van Gastel et al. (1985) found that the shape of the mean velocity profile can change the growth rate by a factor of more than three. In addition, the perturbation equations are sensitive to the details of the turbulence profiles in the vicinity of the air-water interface. Given the sensitivity of the perturbation problem to the mean profiles, it is essential that the mean flow equations are solved through both boundary layers at the air-water interface.

The solution of the mean flow problem is developed for the case of a stratified

two-phase (air-water) flow in the the Stanford Wind Water Wave Research Facility (SWWWRF) for several reasons. First, this will allow comparisons of the mean flow profiles with previous experimental measurements in the SWWWRF. Second, this will also allow comparisons of both mean and wave-induced quantities with the results of our ongoing particle tracking experiments in the SWWWRF. Third, other test cases of interest (e.g., fully developed boundary layer with no pressure gradient) are easily computed as simplifications of the two-phase channel flow problem.

As it turns out, the mean flow equations are quite challenging to solve numerically, since they are non-linear and involve very steep gradients near the boundaries and the interface. Indeed, we speculate that the difficulty of solving the coupled mean flow equations for the "long wave" domain has hindered previous efforts to extend the success of the "short wave" models of Valenzuela, Kawai, and van Gastel et al. However, we are hopeful that the considerable effort involved in solving these equations will pay dividends in the long run, and that the solution of the perturbation equations using the computed mean profiles will yield growth rates in better agreement with experiments.

The following sections discuss details of the formulation of the model, the numerical solution techniques, and results obtained from comparisons of the mean flow model to several test cases.

2 Mathematical Formulation

2.1 Governing equations and turbulence model

The numerical model solves for the turbulent, stratified air-water flow in a channel. The flow field is perturbed by a two-dimensional, monochromatic, small amplitude gravity wave at the interface. In addition, depending on the windspeed, the interface may be ruffled by short wavelength wind-generated ripples. These ripples are treated as roughness at the interface. The model is based on the Continuity equation, the Reynolds averaged Navier-Stokes equations, and two transport equations for the turbulent kinetic energy and the dissipation which are necessary to provide closure for the unknown Reynolds stress terms which appear in the Navier-Stokes equations. These equations are transformed to the wavy coordinate system of Hsu et al. (1981) so that the water surface becomes a straight line. The transform greatly facilitates the application of the coupling conditions at the air-water interface. In fact, Norris and Reynolds (1975) found that such a transform was essential to obtain good agreement between their experiments and their numerical model. The transformed equations are then expanded in terms of the wave slope, ak, where a is the wave amplitude, $k = 2\pi/L$ is the wave number, and L is the wave length. Terms of order $(ak)^0$ in the resulting equations describe the mean flow over the wavy interface, while terms of order $(ak)^1$ describe the first order perturbations to the mean flow. As it turns out, the zeroth order mean flow equations in the transformed coordinate system are identical to the governing equations for stratified two-phase

flow in a channel with no gravity wave present on the interface. Thus, the details of the coordinate transformation are not presented here. It suffices to point out that the solution is valid either in an untransformed (cartesian) coordinate system with no wave at the interface, or in the transformed coordinate system.

The model assumes that both fluids are incompressible with constant physical properties and that the flow is steady, turbulent, and fully developed. In our experimental facility the mean flow does change slightly with fetch. However, the assumption of fully developed flow is justified in our case since in reality the mean flow profile changes only very slightly over one wavelength of the gravity wave at the interface. The well known k-epsilon turbulence model is used to model the turbulence in the flow. Since the perturbation equations have been found to be very sensitive to the mean velocity profile, it is essential that the mean profile be computed through the boundary layers at the air-water interface, rather than using empirical wall functions applied at some distance above the interface. The standard k-epsilon is only valid for regions where molecular viscosity is unimportant (i.e., far from the boundaries and the interface). Thus, we have used an extended version of the standard k-epsilon model that is valid for low Reynolds number regions. We decided to use the model proposed by Launder and Sharma (1974) since Patel et al. (1984) found that it performed among the best of the models they evaluated in a variety of test cases. This model has also been successfully applied to similar stratified two-phase flow problems by Akai et al (1981) and Issa (1988).

The equations governing the mean flow in both fluids for steady, fully developed flow are (Patel et al., 1985)

$$\frac{\partial}{\partial y}\left[(\nu+\nu_T)\frac{\partial u}{\partial y}\right]-\frac{1}{\rho}\frac{\partial p}{\partial x}=0 \tag{1}$$

$$\frac{\partial}{\partial y}\left[\left(\nu+\frac{\nu_T}{\sigma_k}\right)\frac{\partial k}{\partial y}\right]+\nu_T\left(\frac{\partial u}{\partial y}\right)^2-\epsilon=0 \tag{2}$$

$$\frac{\partial}{\partial y}\left[\left(\nu+\frac{\nu_T}{\sigma_\epsilon}\right)\frac{\partial \tilde{\epsilon}}{\partial y}\right]+c_{1\epsilon}f_1\frac{\tilde{\epsilon}}{k}\nu_T\left(\frac{\partial u}{\partial y}\right)^2-c_{2\epsilon}f_2\frac{\tilde{\epsilon}^2}{k}+g=0 \tag{3}$$

where

$$\nu_T=c_\mu f_\mu\frac{k^2}{\tilde{\epsilon}} \tag{4}$$

$$\epsilon=\tilde{\epsilon}+d \tag{5}$$

$$R_T=\frac{k^2}{\nu\tilde{\epsilon}} \tag{6}$$

$$k=\frac{1}{2}\overline{u_i'u_i'} \tag{7}$$

and

$$\epsilon = \nu \overline{\frac{\partial u_j'}{\partial x_i} \frac{\partial u_j'}{\partial x_i}} \tag{8}$$

In the above equations, y is the vertical coordinate measured upwards from the channel bottom, x is the streamwise coordinate, u is the streamwise velocity, k is the turbulent kinetic energy, and ϵ is the (homogeneous) dissipation rate. Also, ν represents the kinematic viscosity, and ρ represents the density. The remaining constants and functions depend on the type of low turbulence Reynolds number model used. These constants and functions are defined below for the Launder-Sharma model:

$$d = 2\nu \left(\frac{\partial \sqrt{k}}{\partial y} \right)^2 \tag{9}$$

$$g = 2\nu\nu_T \left(\frac{\partial^2 u}{\partial y^2} \right)^2 \tag{10}$$

$$f_\mu = \exp\left[\frac{-3.4}{(1 + R_T/50)^2} \right] \tag{11}$$

$$f_1 = 1 \tag{12}$$

$$f_2 = 1 - 0.3 \exp\left(-R_T^2\right) \tag{13}$$

A big advantage of the Launder-Sharma low-Reynolds-number model presented above is that the turbulence Reynolds number, R_T, is the only parameter that determines the behavior of the model near a boundary. As a consequence, it is possible to have a non-zero value of turbulent kinetic energy at a boundary with the Launder-Sharma model. In contrast, many of the other available low R_T models were originally developed for flow near solid walls, and require that the turbulent kinetic energy is zero at the boundaries. While this restriction is true for a solid, smooth wall, it is not necessarily valid for rough boundaries, or the air-water interface.

For high turbulence Reynolds numbers, R_T, the functions f_μ and f_2 tend to unity, and so the behavior of the model depends only on the values of the five remaining constants. The values of these constants are taken to be $c_\mu = 0.09$, $c_{1\epsilon} = 1.44$, $c_{2\epsilon} = 1.92$, $\sigma_k = 1.0$, and $\sigma_\epsilon = 1.3$, which are the same as for the standard high-Reynolds-number k-epsilon turbulence model. Thus, the Launder-Sharma model reduces to the standard k-epsilon model away from the boundaries and the interface.

2.2 Application of the governing equations to two-phase stratified channel flow

In this section the governing equations presented above are applied to the coupled, two-phase, stratified channel flow problem. Let H be the total height of the channel, and define the lower fluid and the upper fluid to be layers 1 and 2 respectively. Let α be the fraction of the channel height occupied by fluid 1. Define the following non-dimensional variables

$$\begin{array}{lll} U = u/u_*, & K = k/u_*^2, & \tilde{E} = \tilde{\epsilon}H/u_*^3 \\ X = x/H, & Y = y/H, & P = p/\rho_2 u_*^2 \end{array} \tag{14}$$

where u_* is the friction velocity in layer 2 at the interface. Substituting the above non-dimensional variables into the governing equations results in the following equations

$$\frac{\partial}{\partial Y}\left[\left(\frac{V}{R}+\bar{\nu}_T\right)\frac{\partial U}{\partial Y}\right] - \frac{1}{\mathcal{P}}\frac{\partial P}{\partial X} = 0 \tag{15}$$

$$\frac{\partial}{\partial Y}\left[\left(\frac{V}{R}+\frac{\bar{\nu}_T}{\sigma_k}\right)\frac{\partial K}{\partial Y}\right] + \bar{\nu}_T\left(\frac{\partial U}{\partial Y}\right)^2 - \tilde{E} - D = 0 \tag{16}$$

$$\frac{\partial}{\partial Y}\left[\left(\frac{V}{R}+\frac{\bar{\nu}_T}{\sigma_\epsilon}\right)\frac{\partial \tilde{E}}{\partial Y}\right] + c_{1\epsilon}f_1\frac{\tilde{E}}{K}\bar{\nu}_T\left(\frac{\partial U}{\partial Y}\right)^2 - c_{2\epsilon}f_2\frac{\tilde{E}^2}{K} + G = 0 \tag{17}$$

where

$$V = \begin{cases} \nu_1/\nu_2 & \text{if } 0 \le Y < \alpha \\ 1 & \text{if } \alpha < Y \le 1 \end{cases} \tag{18}$$

$$\mathcal{P} = \begin{cases} \rho_1/\rho_2 & \text{if } 0 \le Y < \alpha \\ 1 & \text{if } \alpha < Y \le 1 \end{cases} \tag{19}$$

$$\frac{\partial P}{\partial X} = \begin{cases} \frac{\partial P}{\partial X}_1 & \text{if } 0 \le Y < \alpha \\ \frac{\partial P}{\partial X}_2 & \text{if } \alpha < Y \le 1 \end{cases} \tag{20}$$

$$R = \frac{u_* H}{\nu_2}, \quad \bar{\nu}_T = c_\mu f_\mu \frac{K^2}{\tilde{E}} \quad E = \tilde{E} + D \tag{21}$$

$$D = \frac{2V}{R}\left(\frac{\partial\sqrt{K}}{\partial Y}\right)^2, \quad G = \frac{2V\bar{\nu}_T}{R}\left(\frac{\partial^2 U}{\partial Y^2}\right)^2 \tag{22}$$

The quantity $\tilde{E} = \tilde{\epsilon}H/u_*^3$ is the "dissipation variable". We solve a transport equation for $\tilde{E}$ (rather than E) for numerical convenience, since $\tilde{E}$ is a known quantity at a boundary (see Patel et al., 1984).

The sixth order set of ordinary differential equations presented above requires six boundary conditions. The equations also require two auxiliary conditions in order to select the pressure gradients in each layer, as well as appropriate coupling conditions at the interface of layer 1 and 2.

The upper and lower walls may be considered as hydraulically smooth in our facility, so that the boundary conditions at the lower and upper walls are given by

$$K = 0, \quad \tilde{E} = 0, \quad U = 0 \quad \text{at } Y = 0 \text{ and } Y = 1 \tag{23}$$

Coupling conditions are required to relate the variables in layer 1 to those in layer 2 at the interface. For our problem, it is known that both the velocity and stress are continuous across the interface. However, similar relationships are not readily apparent for the turbulent kinetic energy and the dissipation rate (Issa, 1988). Thus, it was decided to solve a quasi-coupled problem in which values of K and $\tilde{E}$ are prescribed at the interface in a similar way to a solid boundary, whereas the velocity and the stress are assumed to be continuous there. The stress and velocity coupling conditions at $Y = \alpha$ are given by
velocity continuity:

$$U_1 = U_2 \tag{24}$$

stress continuity:

$$\left[\mathcal{P}\left(\frac{V}{R} + \bar{\nu}_T\right)\frac{\partial U}{\partial Y}\right]_1 = \left[\mathcal{P}\left(\frac{V}{R} + \bar{\nu}_T\right)\frac{\partial U}{\partial Y}\right]_2 \tag{25}$$

The prescribed values of K and $\tilde{E}$ may be expressed as

$$\begin{aligned} K_1 &= K_{0_W}, \quad K_2 = K_{0_A} \\ \tilde{E}_1 &= \tilde{E}_{0_W}, \quad \tilde{E}_2 = \tilde{E}_{0_A}. \end{aligned} \tag{26}$$

For a smooth interface, K_{0_A}, K_{0_W}, $\tilde{E}_{0_A}$, and $\tilde{E}_{0_W}$ are zero, whereas for a rough interface these values are non-zero. We found that the specification of a non-zero value of turbulent kinetic energy at the interface as used by Akai et al. (1981) and Issa (1988) could not predict the measured velocity profiles in our channel for free stream wind speeds greater than about 3 m/s. Thus, we developed a more rational method for predicting the boundary values of turbulent kinetic energy and dissipation rate at a rough, wavy interface that is applicable to smooth, transitional, and fully rough flow regimes. It is assumed that the interfacial roughness may be characterized by a roughness length, y_0, which is defined as the vertical intercept of a semilogarithmic plot of y versus $u(y) - u_s$, where u_s is the surface drift velocity velocity (Amorocho and DeVries, 1980). Both the water and the air are assumed to be subject to the same roughness elements (Kondo, 1976), so that the roughness Reynolds number in the air is about twice that in the water. Effectively, this means that the interfacial region is treated in a similar manner to a solid boundary. That is, all effects of the orbital motions of the water waves have been ignored for the present time.

The values of K and $\tilde{E}$ at the interface may be determined by ensuring that the eddy viscosity at the wall (given by Equation [21]) is consistent with that predicted by the mixing length model, as well as by a one-equation turbulence model. The eddy viscosity for the mixing length model is given (in non-dimensional form) by

$$\bar{\nu}_T = L^2\frac{\partial U}{\partial Y} \tag{27}$$

(Kays and Crawford, 1980), whereas the eddy viscosity for a one-equation turbulence model is given by

$$\bar{\nu}_T = c_\mu^{1/4} \sqrt{K} L \tag{28}$$

(ASCE Task Committee on Turbulence Models in Hydraulic Computations, 1988) where L is the turbulent length scale (or mixing length). By noting that $L_0 = \kappa y_0 / H$ at the interface ($Y = \alpha$) and eliminating $\bar{\nu}_T$ from Equations [21], [27], and [28], the following expressions for K_0 and $\tilde{E}_0$ are obtained

$$K_0 = \frac{1}{4L_0^2\sqrt{c_\mu}} \left(-V/R + \sqrt{(V/R)^2 + 4L_0^2/\mathcal{P}} \right) \tag{29}$$

$$\tilde{E}_0 = c_\mu^{3/4} K_0^{3/2} f_\mu(K_0, \tilde{E}_0)/L_0. \tag{30}$$

Thus, if the non-dimensional roughness height, $Y_0 = y_0/H$, is known, the values of K_0 and $\tilde{E}_0$ on either side of the interface (i.e., K_{0_W}, K_{0_A}, $\tilde{E}_{0_W}$ and $\tilde{E}_{0_A}$) may be determined. In practice, the roughness height, y_0, may be related to the free stream wind speed and the friction velocity, u_* (Amorocho and DeVries, 1980).

The values of K_0 and $\tilde{E}_0$ predicted from Equations [29] and [30] have the correct assymptotic behavior. That is, for $Y_0 \to 0$ (i.e., smooth boundary) they yield $K_0 = 0$ and $\tilde{E}_0 = 0$ at the interface, whereas for large Y_0 (i.e., fully rough flow) they predict $K_0 \to 1/(\mathcal{P}\sqrt{c_\mu})$ and $\tilde{E}_0 \to 1/(\kappa Y_0 \mathcal{P}^{3/2})$, which are exactly the wall functions applied at $Y = Y_0$ (ASCE Task Committee on Turbulence Models in Hydraulic Computations, 1988). Thus, they provide a general method for specifying boundary conditions on the turbulent kinetic energy and the dissipation rate at a smooth, transitional, or rough boundary.

Finally, conditions are required to set the pressure gradients in each layer. For fully developed channel flow the pressure gradient in each layer must be a constant value. However, these pressure gradients are initially unknown. Also, since the flow in each layer is coupled, the pressure gradient in layer 1 affects the flow in layer 2 and vice versa. Since there is no net flow in the lower layer for a laboratory facility such as the SWWWRF, the pressure gradients must be chosen such that the average velocity (i.e., flow rate) in layer 1 is zero. Another condition that must be satisfied by the solution is that the non-dimensional stress at the interface in layer 2 must be unity (this is a consequence of normalizing the solution on the friction velocity at the interface in layer 2). These conditions may be expressed as

$$\int_0^\alpha U(Y)\, dY = 0 \tag{31}$$

$$\left[\mathcal{P} \left(\frac{V}{R} + \bar{\nu}_T \right) \frac{\partial U}{\partial Y} \right]_2 = 1 \text{ at } Y = \alpha \tag{32}$$

Given the above condition on the stress at the interface, Equation [15] may be integrated to yield

$$\bar{\tau}(Y) = \frac{\partial P}{\partial X}(Y - \alpha) + 1 \tag{33}$$

where

$$\bar{\tau} = \mathcal{P}\left(\frac{V}{R} + \bar{\nu}_T\right)\frac{\partial U}{\partial Y} \tag{34}$$

is the total shear stress normalized by $\rho_2 u_*^2$. This integration reduces the order of the equation set by one. Since the auxiliary condition relating to the stress at the interface has been used, the new auxiliary condition on the choice of pressure gradient is chosen to be the boundary condition $U(1) = 0$.

3 Numerical solution

The governing equations to be solved are a 5th order set of non-linear ordinary differential equations. Along with the boundary and coupling conditions, they comprise a 3 point boundary value problem (BVP). In our case the problem is a difficult one, since it involves the computation of profiles through four boundary layers - one at each wall, and two at the air-water interface. In addition, the low-Reynolds-number k-epsilon model introduces increased computational difficulty.

Initially, we attempted to solve the problem using the shooting method. This method had been successfully applied to a simpler channel flow problem by Norris and Reynolds (1975), who used a one-equation turbulence model. Briefly, this method involves guessing unknown boundary conditions at the channel bottom, then integrating (or shooting) toward the top wall where the known boundary conditions are checked. If the top wall boundary conditions are not satisfied, then a new guess is made for the bottom boundary values, and the process continues until the top wall boundary conditions are satisfied. Unfortunately, the governing equations proved extremely sensitive to small changes in the two unknown bottom boundary conditions (i.e., the equations are very stiff in the mathematical sense), and so the shooting method failed for our problem. On the other hand, Norris and Reynolds only had one unknown boundary condition at the channel bottom; thus, it was possible to use the shooting method effectively in their case, even though their problem was still very sensitive to the unknown boundary condition.

Next, the equations were solved by the method of Patankar and Spalding (1967) for parabolic partial differential equations. This method involved reintroducing the time derivatives into the governing equations, finite differencing the resulting partial differential equations, then marching forward in time from an initial guess to steady state. The time marching technique chosen is second-order accurate and implicit, so that the method is unconditionally stable. In our case the non-linear equations must be linearized at each step. In practice, this linearization limits the time step that can be used to achieve convergence to a small value. If larger time steps are used, the solution may become non-physical (e.g., negative values of k and ϵ). This method of solution proved to give satisfactory results. However, the rate of convergence towards steady state is extremely slow in some cases, and a large number of iterations (e.g., 10,000 to 20,000) are required to reach steady state. This slow rate of convergence was also found by Akai et al. (1981) who used a similar

time marching method to solve the stratified two-phase flow problem, and found that about 10000 iteration cycles were required to reach steady state.

Finally, the problem was solved using a conceptually simple finite difference method for non-linear BVPs outlined by Ascher et al. (1988). With this technique, an initial guess at the solution is updated iteratively, using Newton iteration, until convergence is achieved. This method has been found to give extremely rapid convergence to the final solution (theoretically, the convergence is quadratic). For example, given a suitable initial guess, the problem converges to the solution in only 10 to 20 iterations. The excellent convergence properties of Newton's method do not come without a price, however. First, the method requires the specification of the Jacobian matrix which involves very complicated algebraic expressions for our particular problem. Second, the method requires a good initial guess to the solution (a known characteristic of Newton's method). Fortunately, a good initial guess was available in our case, since we had already solved the problem using the time-marching technique. Once a solution was obtained for one test case (e.g., for a given Reynolds number), it was used as an initial guess for related test cases. Details of the application of the finite difference method with Newton iteration to our problem are presented in the following section.

3.1 Reduction of the problem to a set of first order ODEs

The BVP was reduced to a coupled set of first order ODEs for solution by the finite difference technique. This reduction has two main advantages. First, the gradients of the principal variables (i.e., U, K, and $\tilde{E}$) are obtained from the solution, as well as the principal variables themselves. Since the perturbation equations require mean profiles and their first and second derivatives, this means our numerical profiles only have to be differentiated numerically once, instead of twice, thus eliminating one possible source of error. Second, the reduction technique greatly facilitates the application of gradient (Neumann) boundary conditions and coupling conditions, which were used for some test cases.

By defining $\lambda_U = V/R + \bar{\nu}_T$, $\lambda_K = V/R + \bar{\nu}_T/\sigma_k$, and $\lambda_E = V/R + \bar{\nu}_T/\sigma_\epsilon$, we may write the above equations as

$$\mathbf{z}' = \mathbf{f}(Y, \mathbf{z}) \quad 0 < Y < 1 \tag{35}$$

where

$$\mathbf{z} = \left\{K, \tilde{E}, U, A, B\right\}^T \tag{36}$$

$$\mathbf{f} = \{A/\lambda_K, B/\lambda_E, C/\lambda_U, -S_K, -S_E\}^T \tag{37}$$

and

$$S_K = \bar{\nu}_T \left(\frac{C}{\lambda_U}\right)^2 - \tilde{E} - D \tag{38}$$

$$S_E = c_{1\epsilon} f_1 \frac{\tilde{E}}{K} \bar{\nu}_T \left(\frac{C}{\lambda_U}\right)^2 - c_{2\epsilon} f_2 \frac{\tilde{E}^2}{K} + G \tag{39}$$

$$A = \lambda_K \frac{\partial K}{\partial Y} \tag{40}$$

$$B = \lambda_E \frac{\partial \tilde{E}}{\partial Y} \tag{41}$$

$$C = \lambda_U \frac{\partial U}{\partial Y} \tag{42}$$

The above equations are solved using the distribution of $C(Y)$ found from Equation [33], along with boundary, coupling, and auxiliary conditions given by Equations [23] to [32].

3.2 Finite difference method

The finite difference method with Newton iteration for non-linear problems given by Ascher et al (1988) is presented below, using their notation. Consider our non-linear boundary value problem (BVP) of order $N = 5$ given by

$$\mathbf{z}' = \mathbf{f}(Y, \mathbf{z}) \quad 0 < Y < 1 \tag{43}$$

with boundary conditions

$$\mathbf{g}(\mathbf{z}(0), \mathbf{z}(1)) = \mathbf{0} \tag{44}$$

For numerical approximation consider a mesh represented by

$$\pi : 0 = Y_1 < Y_2 < \ldots < Y_{M+1} = \alpha = Y_{M+2} < \ldots < Y_{2M+2} = 1 \tag{45}$$

where $1 \leq i \leq M+1$ for layer 1, and $M+2 \leq i \leq 2M+2$ for layer 2. The points $M+1$ and $M+2$ are the interfacial grid points in layer 1 and 2, respectively. Denote the vector of approximate solution values at the mesh points by $\mathbf{z}_\pi$.

A one-step scheme (i.e., a scheme in which the difference operator is based only on values related to one subinterval of the mesh at a time) is used to represent the derivative term. One-step schemes have the considerable advantage over the more conventional (at least in fluid mechanics) two-step schemes in that the order of accuracy of the finite difference method is preserved for a non-uniform grid. That is, if the one-step scheme is second order, the finite difference equations will also be second order, regardless of whether the grid spacing is uniform or not. Two of the most well known one-step methods are the midpoint scheme and the trapezoidal method, which are both second order accurate. Our BVP exhibits a mild singularity at the boundaries, since $K = 0$ and $\tilde{E} = 0$ results in $\bar{\nu}_T$, D and, hence, $\mathbf{f}$ being undefined. Thus, for our problem, the midpoint scheme is particularly appropriate, since it does not actually evaluate the vector $\mathbf{f}$ at the grid points - only in between. Application of the midpoint scheme to the ODE yields

$$\frac{\mathbf{z}_{i+1} - \mathbf{z}_i}{h_i} = \mathbf{f}(Y_{i+1/2}, \frac{1}{2}(\mathbf{z}_i + \mathbf{z}_{i+1})) \tag{46}$$

with boundary conditions given by

$$\mathbf{g}(\mathbf{z}_1, \mathbf{z}_{2M+2}) = \mathbf{0} \tag{47}$$

where $Y_{i+1/2} = Y_{i+1} - Y_i$. Since there is a discontinuity in the fluid properties at the interface, the finite difference equation above does not hold for the grid point $i = M + 1$. Instead, analytical relationships (i.e., the coupling conditions) relate the interfacial variables in layer 1 to those in layer 2.

Equations [46] and [47], along with the interfacial coupling conditions, represent a system of $N(2M + 2)$ non-linear equations for the $N(2M + 2)$ unknowns, $\mathbf{z}_\pi$. Newton's method is used to solve the non-linear system. Application of Newton's iteration method to the above non-linear problem results in (see Ascher et al. (1988))

$$\frac{\mathbf{w}_{i+1} - \mathbf{w}_i}{h_i} - \frac{1}{2}\left[A(Y_{i+1/2})\mathbf{w}_{i+1} + A(Y_{i+1/2})\mathbf{w}_i\right] = -N_\pi \mathbf{z}_i^m \tag{48}$$

where

$$N_\pi \mathbf{z}_i^m = \frac{\mathbf{z}_{i+1} - \mathbf{z}_i}{h_i} - \mathbf{f}(Y_{i+1/2}, \frac{1}{2}(\mathbf{z}_i + \mathbf{z}_{i+1})) \tag{49}$$

$$A(Y_{i+1/2}) = \frac{\partial \mathbf{f}}{\partial \mathbf{z}}\left(Y_{i+1/2}, \frac{1}{2}(\mathbf{z}_i + \mathbf{z}_{i+1})\right) \tag{50}$$

Here $\mathbf{z}_\pi^m$ is the known solution after m iterations ($\mathbf{z}_\pi^0$ is the initial guess). The boundary conditions at the lower and upper walls may be written as

$$B_a \mathbf{w}_1 + B_b \mathbf{w}_{2M+2} = -\mathbf{g}(\mathbf{z}_1^m, \mathbf{z}_{2M+2}^m) \tag{51}$$

where

$$B_a = \frac{\partial \mathbf{g}(\mathbf{z}_1^m, \mathbf{z}_{2M+2}^m)}{\partial \mathbf{z}_1^m} \tag{52}$$

and

$$B_b = \frac{\partial \mathbf{g}(\mathbf{z}_1^m, \mathbf{z}_{2M+2}^m)}{\partial \mathbf{z}_{2M+2}^m} \tag{53}$$

The next iterate is determined by

$$\mathbf{y}_i^{m+1} = \mathbf{y}_i^m + \mathbf{w}_i \tag{54}$$

The linear system represented by Equation [48] may be written as

$$S_i \mathbf{w}_i + R_i \mathbf{w}_{i+1} = \mathbf{q}_i \tag{55}$$

where S_i and R_i are the $N \times N$ matrices

$$S_i = -h_i^{-1} I - \frac{1}{2} A(Y_{i+1/2}) \tag{56}$$

$$R_i = h_i^{-1} I - \frac{1}{2} A(Y_{i+1/2}), \tag{57}$$

and q_i is the right hand side vector formed from the currently available solution vector $\mathbf{z}_i^m$ given by

$$\mathbf{q}_i = -N_\pi \mathbf{z}_i^m. \tag{58}$$

For our problem the boundary conditions at the upper and lower walls are separated. Suppose there are nu boundary condtions at the upper boundary. Then, there must be $nl = N - nu$ boundary conditions at the lower boundary (for our problem $nu = 2$ and $nl = 3$). By selecting the appropriate rows from the matrices B_a and B_b the boundary conditions may be expressed as

$$B_l \mathbf{w}_1 = -\mathbf{g}_l(\mathbf{z}_1^m) \tag{59}$$

and

$$B_u \mathbf{w}_{2M+2} = -\mathbf{g}_u(\mathbf{z}_{2M+2}^m) \tag{60}$$

where B_u is an $nu \times N$ matrix, B_l is an $nl \times N$ matrix, g_u is a vector of length nu, and g_l is a vector of length nl. Finally, the coupling conditions at the interface may be written as

$$S_\alpha \mathbf{w}_{M+1} + R_\alpha \mathbf{w}_{M+2} = \mathbf{q}_\alpha \tag{61}$$

The detailed matrix structure of the linear system is shown below:

$$\begin{pmatrix} B_l & & & & & & & & \\ S_1 & R_1 & & & & & & & \\ & S_2 & R_2 & & & & & & \\ & & \cdot & & & & & & \\ & & & \cdot & & & & & \\ & & & & S_\alpha & R_\alpha & & & \\ & & & & & \cdot & & & \\ & & & & & & \cdot & & \\ & & & & & & S_{2M+1} & R_{2M+1} & \\ & & & & & & & B_u & \end{pmatrix} \begin{pmatrix} \mathbf{w}_1 \\ \mathbf{w}_2 \\ \cdot \\ \cdot \\ \cdot \\ \mathbf{w}_{M+1} \\ \mathbf{w}_{M+2} \\ \cdot \\ \mathbf{w}_{2M+1} \\ \mathbf{w}_{2M+2} \end{pmatrix} = \begin{pmatrix} -\mathbf{g}_l \\ \mathbf{q}_1 \\ \mathbf{q}_2 \\ \cdot \\ \cdot \\ \mathbf{q}_\alpha \\ \cdot \\ \cdot \\ \mathbf{q}_{2M+1} \\ -\mathbf{g}_u \end{pmatrix} \tag{62}$$

For compactness, this equation is expressed as

$$\hat{A} \mathbf{w}_\pi = \hat{\beta} \tag{63}$$

3.3 Solution algorithm

At each iteration step, Equation [63] above must be solved to obtain the vector $\mathbf{w}_\pi$. One method of solving the large staircase matrix, $\hat{A}$, is to consider it as banded, with a lower bandwidth of $N + nl - 1$, and an upper bandwidth of $N + nu - 1$.

Gaussian elimination requires an increase in the upper bandwidth to $2N-1$, and so storing the matrix requires an array of size $N(2M+2) \times (3N+nl-1)$. This means that the storage requirements, as well as the computational effort required to solve the matrix are optimally linear in the number of grid points, $2M+2$. Although there are more efficient methods available to solved this staircase matrix (Ascher et al., 1988, Chapter 7), the banded method was chosen since routines to solve banded matrices are readily available in standard subroutine libraries. For our problem, the routines DGBFA and DGBSL from the LINPACK subroutine library were used to factor and solve the banded matrix at each step in the solution procedure.

Given a Reynolds number, R, and two trial pressure gradients, $\frac{\partial P}{\partial X}_1$ and $\frac{\partial P}{\partial X}_2$, the solution to the boundary value problem may be found using the following algorithm (Ascher et al., 1988, Chapter 5).

1. Generate a mesh, π, and an initial guess, $\mathbf{z}_\pi^0$. Decide on a solution tolerance, TOL.

REPEAT

2. Generate B_u, B_l, g_u, and g_l.
3. FOR $i = 1, \ldots, 2M+1$ DO
   IF $i = \alpha$ THEN
      Generate S_α, R_α, and $\mathbf{q}_\alpha$
   ELSE
      Generate S_i, R_i, and $\mathbf{q}_i$
4. Solve $\hat{A}\mathbf{w}_\pi = \hat{\beta}$ for $\mathbf{w}_\pi$.
5. FOR $i = 1, \ldots, 2M+1$ DO
   $\mathbf{y}_i^{m+1} = \mathbf{y}_i^m + \mathbf{w}_i$

UNTIL $|\mathbf{w}_\pi| \leq TOL$.

For our problem the solution tolerance was set to 10^{-6} or less. This value is somewhat conservative as the changes in the solution were negligible for values of $|\mathbf{w}_\pi|$ less than about 10^{-3}. However, only one or two iterations were required to reduce the value of $|\mathbf{w}_\pi|$ from 10^{-3} to 10^{-6}, since the convergence of the method is approximately quadratic.

The most difficult part of the solution solution procedure for our problem is the determination of the Jacobian matrix, A, defined by Equation [50], since some components of $\mathbf{f}$ involve the solution variables $\mathbf{z}$ in a very complicated manner. The derivative terms which comprise the 5×5 matrix A were evaluated using the symbolic manipulation program *Mathematica*^{TM}, which greatly simplified the process. The resulting algebraic derivative expressions were output from *Mathematica*^{TM} in FORTRAN form and incorporated directly into a subroutine so that translation errors were avoided.

For the boundary conditions presented in Section 2.2 the boundary condition vector, $\mathbf{g}$, may be written as

$$\mathbf{g} = \left\{K(0), K(1), \tilde{E}(0), \tilde{E}(1), U(0)\right\}^T \tag{64}$$

and the solution vectors at the boundaries are

$$\mathbf{z}_1 = \left\{K(0), \tilde{E}(0), U(0), A(0), B(0)\right\}^T \tag{65}$$

$$\mathbf{z}_{2M+2} = \left\{K(1), \tilde{E}(1), U(1), A(1), B(1)\right\}^T \tag{66}$$

Thus, the boundary condition matrices are given by

$$B_a = \begin{pmatrix} 1 & 0 & 0 & 0 & 0 \\ 0 & 0 & 0 & 0 & 0 \\ 0 & 1 & 0 & 0 & 0 \\ 0 & 0 & 0 & 0 & 0 \\ 0 & 0 & 1 & 0 & 0 \end{pmatrix} \tag{67}$$

and

$$B_b = \begin{pmatrix} 0 & 0 & 0 & 0 & 0 \\ 1 & 0 & 0 & 0 & 0 \\ 0 & 0 & 0 & 0 & 0 \\ 0 & 1 & 0 & 0 & 0 \\ 0 & 0 & 0 & 0 & 0 \end{pmatrix} \tag{68}$$

from which the matrices B_l and Bu, and the vectors $\mathbf{g}_l$ and $\mathbf{g}_u$ are readily apparent.

The solution obtained using the above algorithm will not, in general, satisfy the auxiliary conditions given by Equations [23] and [31]. Thus, the pressure gradients are adjusted, and the problem re-solved until the two auxiliary conditions are satisfied. The adjustment of the pressure gradients to meet the auxiliary conditions is analogous to finding the roots of two non-linear equations. This process is formalized as follows. Define the following:

$$\frac{\partial P}{\partial X_1} = x_1 \tag{69}$$

$$\frac{\partial P}{\partial X_2} = x_2 \tag{70}$$

$$f_1(x_1, x_2) = \int_0^\alpha U(Y)dY \tag{71}$$

and

$$f_2(x_1, x_2) = U(1) \tag{72}$$

The problem is to determine (x_1, x_2) such that f_1 and f_2 are zero. The functions f_1 and f_2 may be expanded in a Taylor series as

$$f_i(\mathbf{x} + \delta\mathbf{x}) = f_i(\mathbf{x}) + \sum_{j=1}^{2} \frac{\partial f_i}{\partial x_j}\delta x_j \tag{73}$$

Since we want $f_i(\mathbf{x} + \delta\mathbf{x}) = 0$, then we may write

$$\sum_{j=1}^{2} \alpha_{ij}\delta x_j = \beta_i \tag{74}$$

where

$$\alpha_{ij} = \frac{\partial f_i}{\partial x_j} \quad \text{and} \quad \beta_i = -f_i \tag{75}$$

The solution algorithm for finding f_1 and f_2 is as follows. Given an initial guess for (x_1, x_2), the BVP is solved to yield f_1 and f_2. Then, the initial guesses are each perturbed by a small amount, and the problem re-solved to yield the functions $(f_1 + \delta f_1, f_2 + \delta f_2)$ corresponding to $(x_1 + \delta x_1, x_2)$ and $(f_1 + \delta f_1^*, f_2 + \delta f_2^*)$ corresponding to $(x_1, x_2 + \delta x_2)$. The Jacobian terms are estimated as follows:

$$\alpha_{11} = \frac{\partial f_1}{\partial x_1} \approx \frac{\delta f_1}{\delta x_1} \tag{76}$$

$$\alpha_{12} = \frac{\partial f_1}{\partial x_2} \approx \frac{\delta f_1^*}{\delta x_2} \tag{77}$$

$$\alpha_{21} = \frac{\partial f_2}{\partial x_1} \approx \frac{\delta f_2}{\delta x_1} \tag{78}$$

$$\alpha_{22} = \frac{\partial f_2}{\partial x_1} \approx \frac{\delta f_2^*}{\delta x_2} \tag{79}$$

The correction to be applied to the pressure gradients may be determined by solving the linear system given by Equation [74] for the vector $(\delta x_1, \delta x_2)$. The process is repeated until f_1 and f_2 are sufficiently close to zero. For our problem, the adjustment of the pressure gradients to satisfy the auxiliary conditions usually only required about 1 or 2 cycles to reduce the absolute errors in f_1 and f_2 to less than 10^{-3}.

4 Results

4.1 Model parameters and initial conditions

The results of the numerical model presented in the previous sections are compared to experimental results for the case of air-water flow in the Stanford Wind Water Wave Research Facility (SWWWRF). The density and viscosity of air were taken to be 1.2 kg/m^3 and 1.5×10^{-5} m^2 s^{-1} respectively, while those for water were taken to be 1000 kg/m^3 and 1.0×10^{-6} m^2 s^{-1}. These values result in the following parameters for the numerical model:

$$\frac{\rho_1}{\rho_2} = 833.3 \tag{80}$$

$$\frac{\nu_1}{\nu_2} = 0.0667 \tag{81}$$

The total channel depth, H, is 1.93 m, and the water depth for the experiments was 0.965 m, so that $\alpha = 0.5$. During the experiments the water surface tilts slightly, causing the reverse pressure gradient in the lower layer, $\frac{\partial P}{\partial X}_1$. However, the change

in water surface level is very small (of the order of a few mm) and so α was set at 0.5 for all cases. Since $\rho_1/\rho_2 \gg 1$ for air-water, the stress at the upper wall and the interface are approximately equal in the air phase. Also, the stress at the lower wall is approximately zero in the water phase. This results in initial estimates of the pressure gradients in the air and water as

$$\frac{\partial P}{\partial X_1} = \frac{1}{\alpha} = 2.0 \tag{82}$$

and

$$\frac{\partial P}{\partial X_2} = \frac{-2}{(1-\alpha)} = -4.0 \tag{83}$$

These pressure gradients are adjusted during program execution using the method described in Section 3.3.

4.2 Comparison of model results with other studies

As discussed in the introduction, Valenzuela (1976) solved the gravity-capillary wave growth problem for a coupled shear flow. He found excellent agreement between his numerical model and experimental investigations of the growth of short waves. One of the key factors in Valenzuela's success was his use of a coupled model which took into account the effect of the shear flow in the water. He used an analytical logarithmic-linear velocity profile to represent the coupled, turbulent mean flow field. In the air the profile is given by

$$u(y) = \begin{cases} u_s + u_*^a y/y_0^a & \text{for } y \le y_1^a \\ u_s + u_1^a + 2.5u_*^a(\alpha_a - \tanh\alpha_a/2) & \text{for } y \ge y_1^a \end{cases} \tag{84}$$

and in the water the profile (in which y is positive into the water) is given by

$$u(y) = \begin{cases} u_s - u_*^w y/y_0^w & \text{for } y \le y_1^w \\ u_s - u_1^w - 2.5u_*^w(\alpha_w - \tanh\alpha_w/2) & \text{for } y \ge y_1^w \end{cases} \tag{85}$$

where

$$\begin{array}{cc} \sinh\alpha_a = (y - y_1^a)/1.25y_0^a & \sinh\alpha_w = (y - y_1^w)/1.25y_0^w \\ y_0^a = \nu_a/u_*^a & y_0^w = \nu_w/u_*^w \end{array} \tag{86}$$

In the above equations, u_s represents the drift velocity at the interface, and superscripts "a" and "w" refer the to air and water, respectively. Valenzuela used $u_s/u_*^a = 0.8$ (i.e., $u_s/u_*^w = 23.1$), and considered two profiles specified by $y_1/y_0 = 5$ and $y_1/y_0 = 8$.

Figure 1 shows a comparison of Valenzuela's mean velocity profile in the water with the numerical model results for the case of a smooth interface and $u_\infty = 1.5$ m/s. The agreement between the numerical results and the analytical profile is excellent. The small difference between the numerical model and the analytical profile near the interface is because the model predicts $u_s/u_*^a = 0.77$ instead of 0.8 used by Valenzuela. If Valenzuela's model is corrected for the drift velocity, it turns

out that the numerical profile falls between the two cases chosen by Valenzuela, which indicates that the Valenzuela profiles were appropriate bounds to the actual profile. The agreement with Valenzuela's profile is encouraging. In fact, one might argue that the coupled numerical model is wasted since the numerical results are so close to the assumed profile of Valenzuela. However, this is not the case. The reason is that, for gravity wave growth, turbulence effects are important (as opposed to the growth of gravity-capilliary waves simulated by Valenzuela). Thus, the perturbation equations require mean profiles of turbulent kinetic energy and dissipation as input, in addition to the mean velocity profile. Analytical expressions for these profiles of mean turbulence quantities are not available, and so our numerical model for the mean flow is essential. In addition, the analytical velocity profile given by Valenzuela does not have continous second derivatives which causes a problem in the perturbation solution.

The numerical model was applied to the coupled air-water flow in the SWWWRF, and the results compared with previously measured experimental data. All the experimental data were measured at a fetch of 13 m from the air inlet. Thus, each experiment may be characterized solely by the free stream wind speed. The measured friction velocities, channel height, and kinematic viscosity of air were used to determine the Reynolds numbers for the simulations. The roughness height, Y_0, was determined from experimental wind profiles using the relationship

$$Y_0 = \frac{z}{H \exp u(z)\kappa/u_*} \tag{87}$$

in which the vertical coordinate z is measured from the air-water interface. The above expression follows directly from the well known logarithmic velocity profile for rough boundaries (Amorocho and DeVries, 1980).

Figure 2 shows a plot of the velocity profile in the air for a free stream wind speed of $U_\infty = 3.2$ m/s, and Figure 3 shows the corresponding velocity profile in the water. The non-zero velocity at the interface may clearly be seen. This drift velocity, u_s, was found to be approximately 3 percent of the wind speed in all cases. The return flow in the water caused by the reverse pressure gradient is also evident in Figure 3. Velocity profiles for other wind speeds are similar to the profiles presented.

The numerical model was used to simulate the experimental results of McIntosh et al. (1975) who measured the velocity profiles above the air-water interface in the SWWWRF using a pitot static tube. Figure 4 shows a comparison of McIntosh's data with the numerical simulation for wind speeds of 2.3 m/s, 3.3 m/s, 5.4 m/s, 8.1 m/s, and 10.7 m/s. The agreement between the numerical model and the experimental points is excellent for the four lowest wind speeds, but the model underpredicts the roughness Reynolds number of the highest wind speeds somewhat. However, the simulation is still within the error bound of the experimental data (about ± 10 percent in u_+), even at the highest wind speed.

Next, the model was used to simulate the experimental results of Cheung (1985, 1988) who measured the velocity profile in the water beneath the air-water interface using a Laser Doppler Anemometer. Figure 5 shows a comparison of Cheung's data

with our model results for 7 wind speeds ranging between 1.5 m/s and 13.1 m/s. The qualitative agreement between the measured and predicted profiles is excellent, showing that the intercept of the profiles decreases with increasing wind velocity as the water surface becomes rougher. The quantitative agreement between the experimental profiles and the numerical simulation may be seen to be quite good for the three highest and the two lowest wind speeds. However, the model does not predict the 3.2 m/s or 4.7 m/s data as well. One reason for the apparent quantitative difference may be attributed to uncertainty in the experimental data. There is a large uncertainty involved in measuring the surface drift velocity which translates into a large uncertainty in the intercept of the experimental profiles in the water. For example, consider the 3.2 m/s case. Cheung quotes an uncertainty of $\pm 10\%$ for u_s which corresponds to 8.4 mm/s. Dividing by the friction velocity, $u_* = 4.9$ mm/s means that the intercept of the 3.2 m/s profiles may be shifted up or down by $u_+ = 1.7$. In addition to this uncertainty, there is at least a $\pm 10\%$ uncertainty in the friction velocity, u_*, and a $\pm 2\%$ error in the velocity measurements themselves. Thus, the combination of these errors results in a large uncertainty in u_+, and so the failure of the expermental profiles to quantitatively agree with the predicted profiles in all cases is not surprising.

It can be seen that the slope of the experimental data in the water deviates from the expected value of $1/\kappa$ for low values of y_+. This deviation is caused by the effects of wave-turbulence interaction (see Howe et al., 1982) disrupting the usual balance of production and dissipation rate that occurs in the vicinity of a solid boundary. Since our numerical model does not consider this effect, the deviation of the experimental data points from the simulation is to be expected for low values of y_+ (i.e., close to the interface).

Figure 6 shows profiles of turbulent kinetic energy predicted by our model in the air above the interface over a range of wind speeds. The model predicts a peak value of k_+ that is somewhat lower than the peak value of $k_+ = 4.5$ suggested by Patel et al. (1985). However, this is a known characteristic of the Launder-Sharma low-Reynolds-number model, and is of little consequence. The increase in turbulent kinetic energy at the interface with wind speed may be clearly identified. The profiles are similar in the water, except that the increase in turbulent kinetic energy at a given wind speed is relatively smaller, since the flow in the water is effectively smoother.

Figure 7 shows corresponding mean profiles of dissipation rate. The characteristic shape of the plot of dissipation rate for a smooth wall is evident, and the profile agrees extremely well with the measured data of Laufer (1954) for the low wind speed (i.e., smooth boundary) case. For higher wind speeds the value of dissipation rate at the interface increases quickly, then begins to decrease with increasing wind speed. Also, the peak in the dissipation rate at about $y_+ = 10$ is gradually reduced as wind speed increases. The model correctly predicts a non-zero value of ϵ at the interface, in contrast to the low turbulent Reynolds number model used by Al-Zanaidi and Hui (1984), which incorrectly yields $\epsilon = 0$ at a boundary.

5 Conclusions

A numerical model of a coupled, stratified, two-phase flow using the k-epsilon turbulence model has been has been presented. The model is efficiently solved numerically using a finite difference technique with Newton iteration. In the development of the model, we have attempted to use well tested methods where possible (e.g., the k-epsilon turbulence model, and the finite difference method of solution).

The numerical model has been applied to the case of the coupled air-water flow in the Stanford Wind Water Wave Research Facility. The agreement between the mean profiles computed by numerical model and experimental data is encouraging. However, the agreement between the simulations and the experimental data somewhat better in the air than in the water. This difference reflects our neglect of the effects of wave-turbulence interaction in the water. Regardless of this deficiency, the model predicts the behavior of the mean profiles quantitatively, as well as qualitatively. In addition, the method for treating the boundary conditions at the air-water interface shows a great deal of promise.

This model has been developed as part of a larger study on the growth of wind-generated waves. The mean profiles generated by the numerical model will be used as input for a linear stability model of wave growth rate. It is anticipated that the inclusion of both the shear flow in the water, and turbulent effects (via the k-epsilon turbulence model) in this model of wave growth will result in improved agreement between predictions and measurements of wave growth rates, especially for long waves.

References

[1] Akai, M., A. Inoue, and S. Aoki, "The prediction of stratified two-phase flow with a two-equation model of turbulence," *Int. J. Multiphase Flow.*, Vol. 7, pp. 21-39, 1981.

[2] Al-Zanaidi, M.A., and W.H. Hui, "Turbulent airflow over water waves - a numerical study," *J. Fluid Mech.*, Vol. 148, pp. 225-246, 1984.

[3] Amorocho, J. and J.J. DeVries, "A new evaluation of the wind stress coefficient over water surfaces," *J. Geophys. Research.*, Vol. 85(C1), pp 433-442, 1980.

[4] Ascher, U.M., R.M.M. Mattheij, and R.D. Russell, "Numerical solution of boundary value problems for ordinary differential equations," Prentice Hall, New Jersey, 1988.

[5] Cheung, T.K., "A study of the turbulent layer in the water at an air-water interface," Ph.D. Dissertation (Technical Report No. 287), Dept. of Civil Eng., Stanford Univ., 1985.

[6] Cheung, T.K., and R.L. Street, "The turbulent layer in the water at an air-water interface," *J. Fluid Mech.*, Vol. 194, pp. 133-151, 1988

[7] Coles, D., "A model for flow in the viscous sublayer," *Proceedings of the workshop on coherent structure of turbulent boundary layers.*, Lehigh University, Bethlehem, Pa., 1978.

[8] Gent, P.R., "A numerical model of the air flow above water waves. Part 2," *J. Fluid Mech.*, Vol. 82(2), pp. 349-369, 1977.

[9] Hsu, C.T., E. Y. Hsu, and R.L. Street, "On the structure of turbulent flows over a progressive water wave: theory and experiment in a transformed, wave-following coordinate system," *J. Fluid Mech.*, Vol. 105, pp. 87-117, 1981.

[10] Issa, R. I., "Prediction of turbulent, stratified, two-phase flow in inclined pipes and channels," *Int. J. Multiphase Flow.*, Vol. 14(2), pp. 141-154, 1988.

[11] Kawai, S., "Generation of initial wavelets by instability of a coupled shear flow and their evolution to wind waves," *J. Fluid Mech.*, Vol. 93(4), pp. 661-703, 1979.

[12] Launder, B.E., and B.I. Sharma, "Application of the energy dissipation model of turbulence to the calculation of a flow near a spinning disk," *Letters in Heat and Mass Transfer.*, Vol. 1, pp. 131-138, 1974.

[13] McIntosh, D.A., R.L. Street, and E.Y. Hsu,"Turbulent heat and momentum transfer at an air-water interface: the influence of surface conditions," Technical Report No. 197, Dept. of Civil Eng., Stanford Univ., 1975.

[14] Miles, J.W., "On the generation of surface waves by shear flows," *J. Fluid Mech.*, Vol. 3, pp. 185-204, 1957.

[15] Miles, J.W., "On the generation of surface waves by shear flows," *J. Fluid Mech.*, Vol. 6, pp. 469-478, 1959.

[16] Norris, H.L., and W.C. Reynolds, "Turbulent channel flow with a moving wavy boundary," Technical Report TF-7, Dept. of Mech. Eng., Stanford Univ., 1975.

[17] Patankar, S.V., and D.B. Spalding., "Heat and mass transfer in boundary layers," Morgan-Grampian, London, 1967.

[18] Patel, V.C., W. Rodi, and G. Scheuerer, "Turbulence models for near-wall and low Reynolds number flows: A review," *AIAA Journal.*, Vol. 23(9), pp. 1308-1319, 1985.

[19] Valenzuela, G.R., "The growth of gravity-capillary waves in a coupled shear flow," *J. Fluid Mech.*, Vol. 76(2), pp. 229-250, 1976.

[20] van Gastel, K., P.A.E.M. Janssen, and G.J. Komen, "On phase velocity and growth rate of wind-induced gravity-capillary waves," *J. Fluid Mech.*, Vol. 161, pp. 199-216, 1985.

[21] Zagustin, K, E.Y. Hsu, and R.L Street, "Turbulent flow over a moving boundary," *Journal of the Waterways and Harbors Division*, ASCE, Vol. 94, No. WW4, Proc. Paper 6210, pp. 397-414, 1968.

Figures

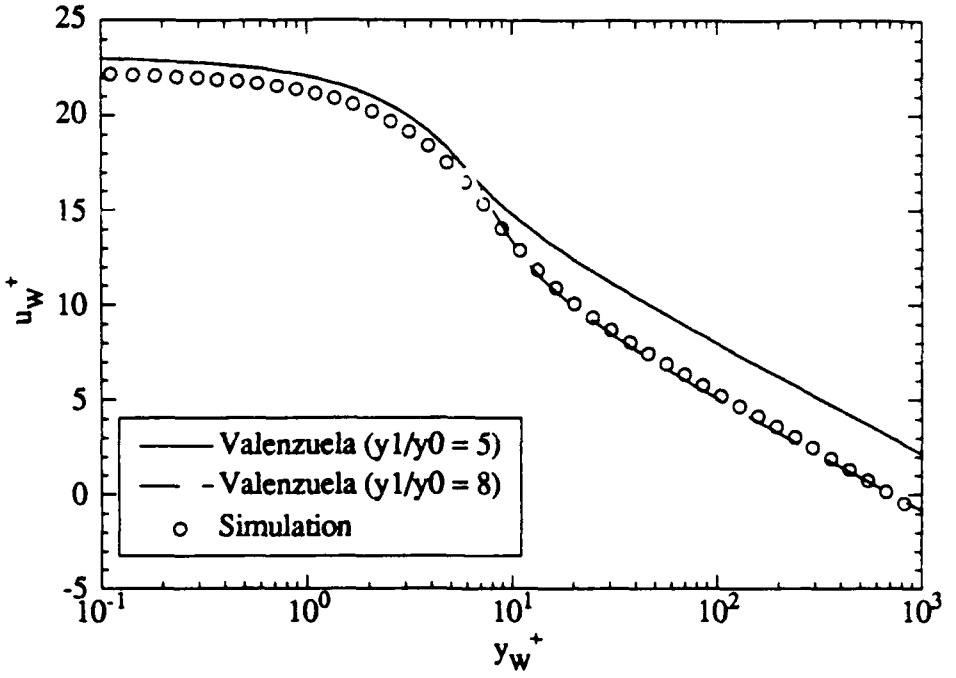

Figure 1: Mean velocity profile beneath interface. Comparison of numerical model and Valenzuela's (1976) profile

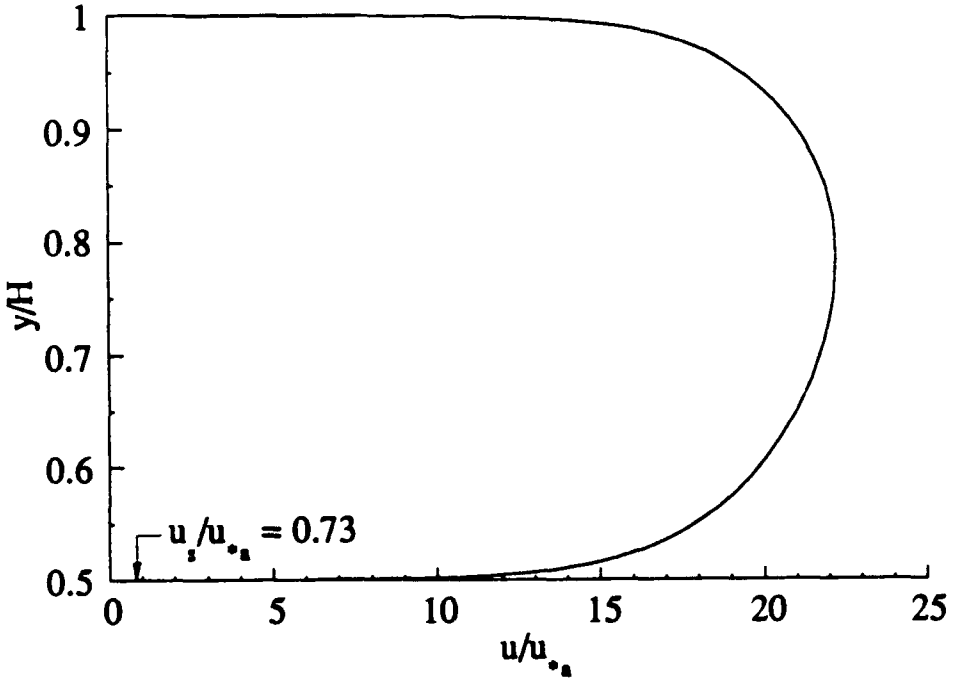

Figure 2: Mean velocity profile in air for $U_\infty = 3.2$ m/s

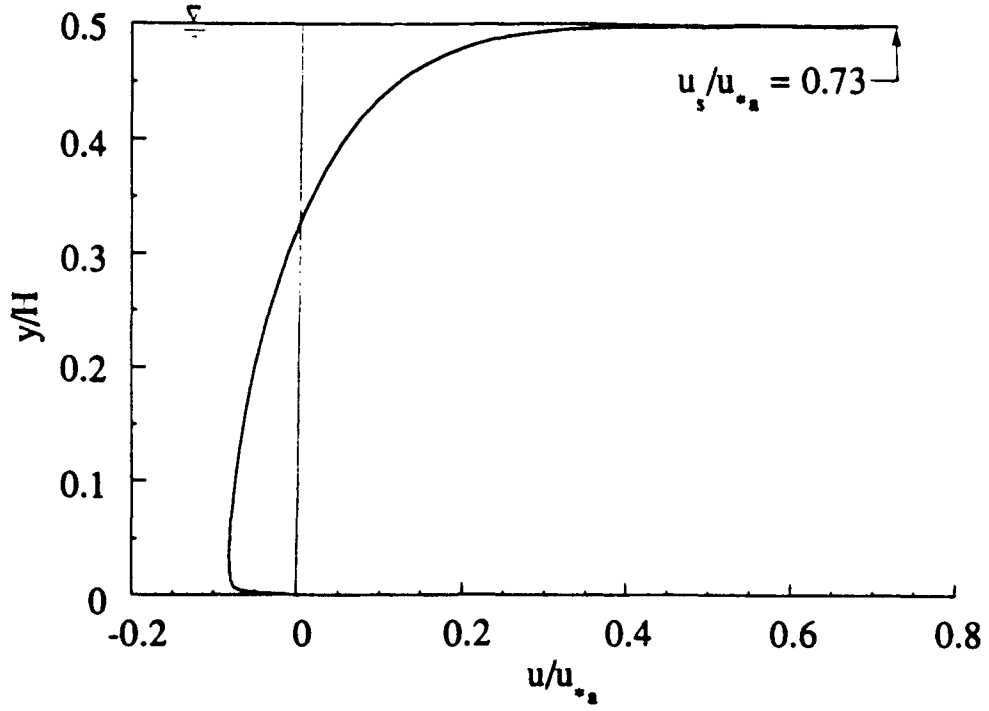

Figure 3: Mean velocity profile in water for $U_\infty = 3.2$ m/s

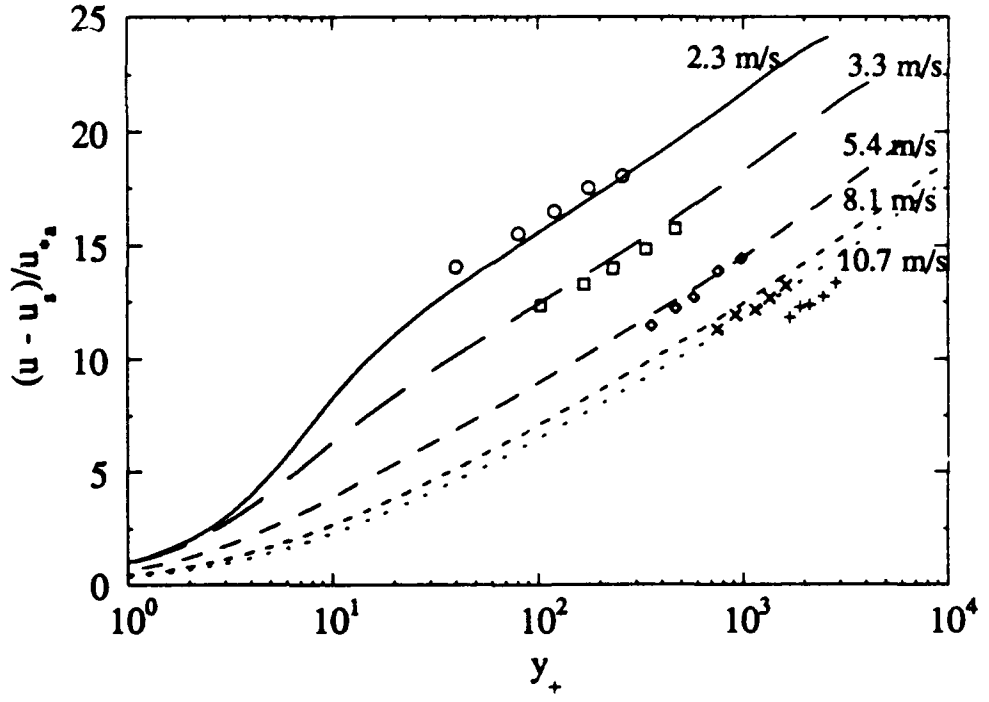

Figure 4: Mean velocity profiles in air above interface. Comparison of numerical model with experiments of McIntosh et al. (1975) data. o - 2.3 m/s; □ - 3.3 m/s; ◇ - 5.4 m/s; × - 8.1 m/s; + - 10.7 m/s

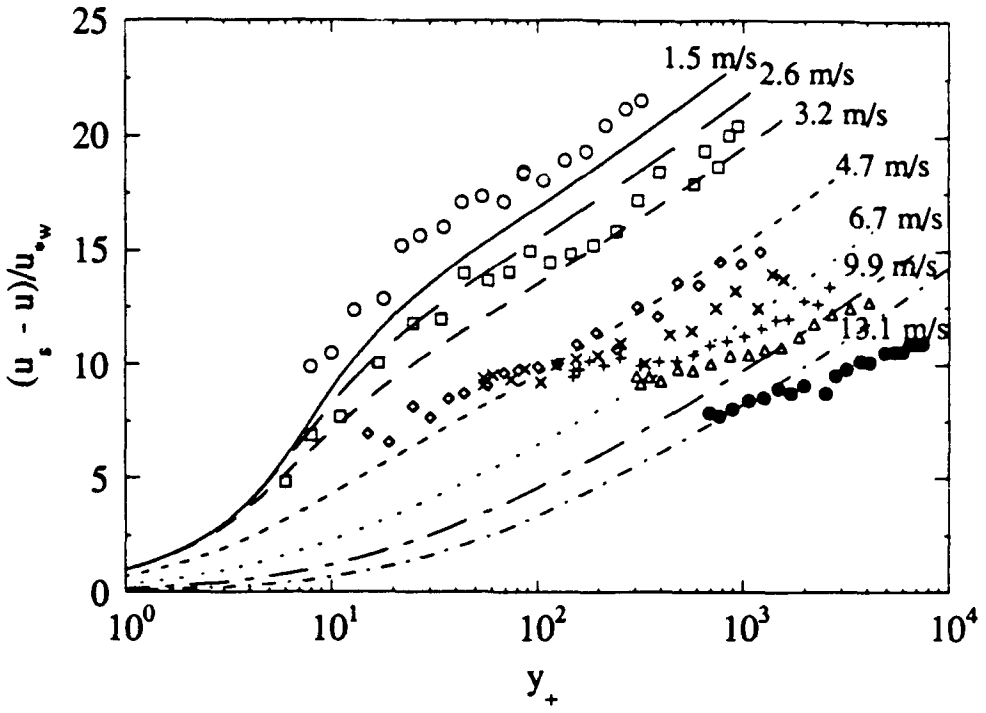

Figure 5: Mean velocity profiles in air above interface. Comparison of numerical model with experiments of McIntosh et al. (1975) data. o - 1.5 m/s; □ - 2.6 m/s; ◇ - 3.2 m/s; × - 4.7 m/s; + - 6.7 m/s; △ - 9.9 m/s; • - 13.1 m/s

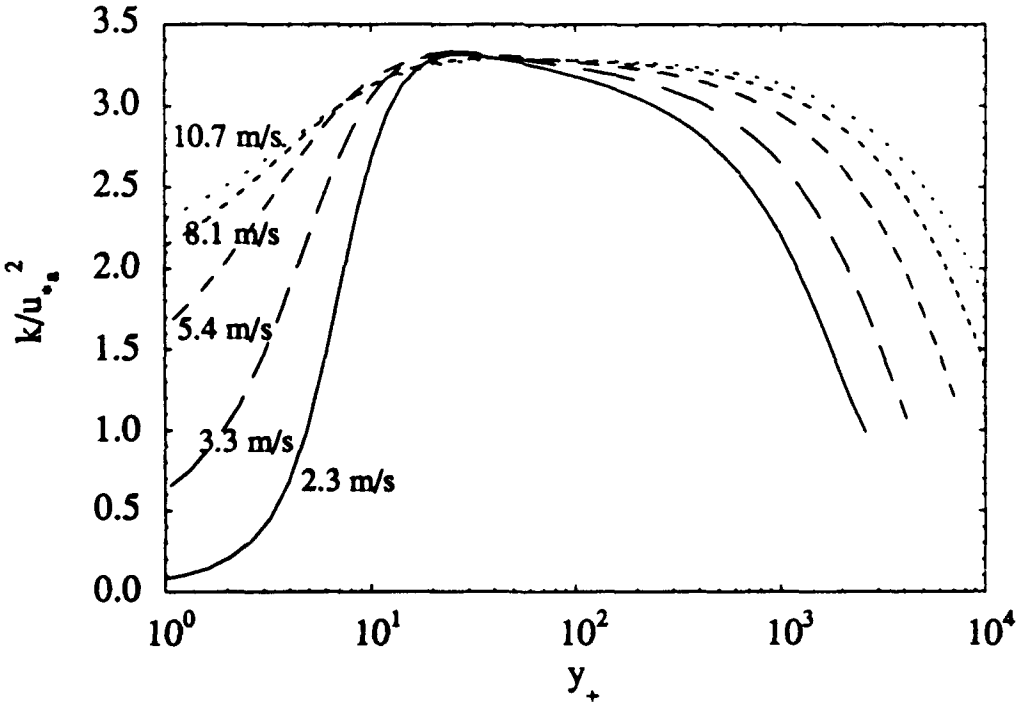

Figure 6: Turbulent kinetic energy profiles in air above interface

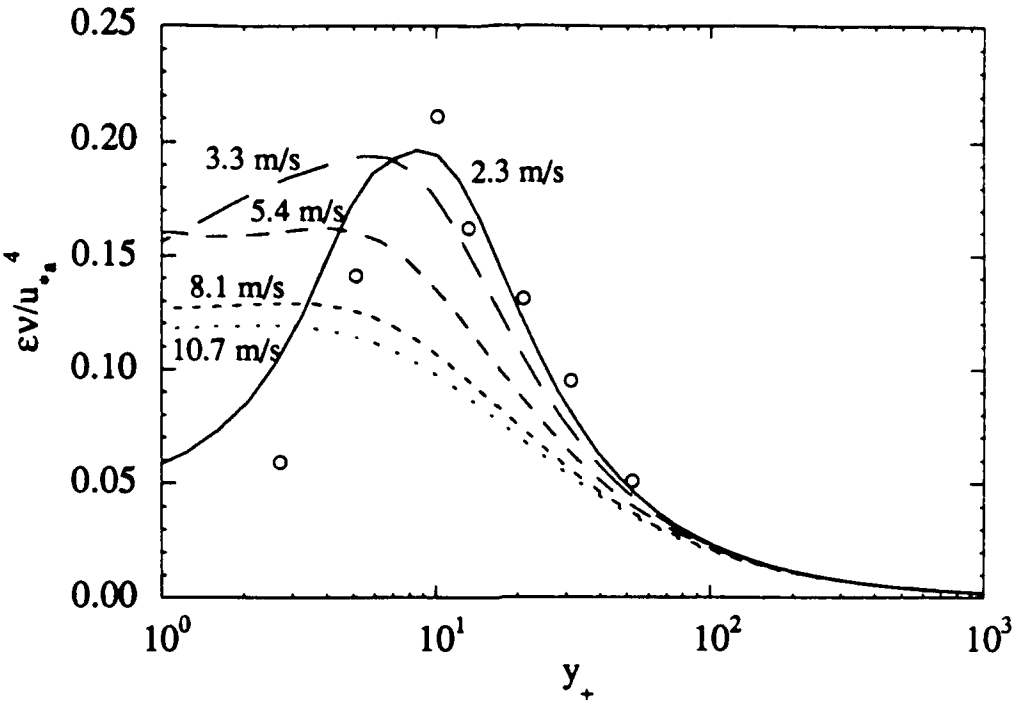

Figure 7: Dissipation rate profiles in air above interface. o - Laufer (1954) data for a smooth wall.

REPORT DOCUMENTATION PAGE

Form Approved
OMB No. 0704-0188

1. AGENCY USE ONLY (Leave blank)	2. REPORT DATE	3. REPORT TYPE AND DATES COVERED
	November 1991	Final Technical 11/15/89 - 2/15/91

4. TITLE AND SUBTITLE

A Study of the Surface Layer at an Air-Water Interface: Solution of Mean Flow Profiles for a Stratified Two-Phase Flow Using the K-Epsilon Turbulence Model

5. FUNDING NUMBERS

Grant
N00014-90-J-1294

6. AUTHOR(S)

Jonathan A. Harris and Robert L. Street

7. PERFORMING ORGANIZATION NAME(S) AND ADDRESS(ES)

Environmental Fluid Mechanics Laboratory
Dept. of Civil Engineering
Stanford University
Stanford, CA 94305-4020

8. PERFORMING ORGANIZATION REPORT NUMBER

EFML 91-1

9. SPONSORING/MONITORING AGENCY NAME(S) AND ADDRESS(ES)

Fluid Dynamics Program ONR
Mechanics Division
Office of Naval Research
800 N. Quincy St., Arlington, VA 22217

10. SPONSORING/MONITORING AGENCY REPORT NUMBER

11. SUPPLEMENTARY NOTES

12a. DISTRIBUTION/AVAILABILITY STATEMENT

Unlimited

12b. DISTRIBUTION CODE

13. ABSTRACT *(Maximum 200 words)*

This is the final technical report on a study of the surface layers at an air-water interface, covering the period 11/15/89 to 2/15/91. A numerical model of a coupled, stratified, two-phase, turbulent flow has been developed as part of a larger study of the growth of waves under wind action. The model has been applied to the case of the coupled air-water flow in the Stanford Wind Water-Wave Research Facility. Comparison of the model results with experiments show that the model predicts mean profiles of velocity, turbulent kinetic energy, and dissipation that are in very good agreement with available data. The mean profiles generated by the model will be used as a basis for a linear-stability model of wave growth.

14. SUBJECT TERMS

Numerical Simulation, Mean Profiles, K-Epsilon Model, Wave Growth

15. NUMBER OF PAGES

26

16. PRICE CODE

17. SECURITY CLASSIFICATION OF REPORT	18. SECURITY CLASSIFICATION OF THIS PAGE	19. SECURITY CLASSIFICATION OF ABSTRACT	20. LIMITATION OF ABSTRACT
Unclassified	Unclassified	Unclassified	

GENERAL INSTRUCTIONS FOR COMPLETING SF 298

The Report Documentation Page (RDP) is used in announcing and cataloging reports. It is important that this information be consistent with the rest of the report, particularly the cover and title page. Instructions for filling in each block of the form follow. It is important to *stay within the lines* to meet *optical scanning requirements*.

Block 1. Agency Use Only *(Leave blank)*.

Block 2. Report Date. Full publication date including day, month, and year, if available (e.g. 1 Jan 88). Must cite at least the year.

Block 3. Type of Report and Dates Covered. State whether report is interim, final, etc. If applicable, enter inclusive report dates (e.g. 10 Jun 87 - 30 Jun 88).

Block 4. Title and Subtitle. A title is taken from the part of the report that provides the most meaningful and complete information. When a report is prepared in more than one volume, repeat the primary title, add volume number, and include subtitle for the specific volume. On classified documents enter the title classification in parentheses.

Block 5. Funding Numbers. To include contract and grant numbers; may include program element number(s), project number(s), task number(s), and work unit number(s). Use the following labels:

C	- Contract	PR	- Project
G	- Grant	TA	- Task
PE	- Program Element	WU	- Work Unit Accession No.

Block 6. Author(s). Name(s) of person(s) responsible for writing the report, performing the research, or credited with the content of the report. If editor or compiler, this should follow the name(s).

Block 7. Performing Organization Name(s) and Address(es). Self-explanatory.

Block 8. Performing Organization Report Number. Enter the unique alphanumeric report number(s) assigned by the organization performing the report.

Block 9. Sponsoring/Monitoring Agency Name(s) and Address(es). Self-explanatory.

Block 10. Sponsoring/Monitoring Agency Report Number. *(If known)*

Block 11. Supplementary Notes. Enter information not included elsewhere such as: Prepared in cooperation with...; Trans. of...; To be published in.... When a report is revised, include a statement whether the new report supersedes or supplements the older report.

Block 12a. Distribution/Availability Statement. Denotes public availability or limitations. Cite any availability to the public. Enter additional limitations or special markings in all capitals (e.g. NOFORN, REL, ITAR).

- DOD - See DoDD 5230.24, "Distribution Statements on Technical Documents."
- DOE - See authorities.
- NASA - See Handbook NHB 2200.2.
- NTIS - Leave blank.

Block 12b. Distribution Code.

- DOD - Leave blank.
- DOE - Enter DOE distribution categories from the Standard Distribution for Unclassified Scientific and Technical Reports.
- NASA - Leave blank.
- NTIS - Leave blank.

Block 13. Abstract. Include a brief *(Maximum 200 words)* factual summary of the most significant information contained in the report.

Block 14. Subject Terms. Keywords or phrases identifying major subjects in the report.

Block 15. Number of Pages. Enter the total number of pages.

Block 16. Price Code. Enter appropriate price code *(NTIS only)*.

Blocks 17. - 19. Security Classifications. Self-explanatory. Enter U.S. Security Classification in accordance with U.S. Security Regulations (i.e., UNCLASSIFIED). If form contains classified information, stamp classification on the top and bottom of the page.

Block 20. Limitation of Abstract. This block must be completed to assign a limitation to the abstract. Enter either UL (unlimited) or SAR (same as report). An entry in this block is necessary if the abstract is to be limited. If blank, the abstract is assumed to be unlimited.